Korean J. Chem. Eng., 34(9), 2507-2513 (2017)
DOI: 10.1007/s11814-017-0161-7

pISSN: 0256-1115
eISSN: 1975-7220

Efficient photocatalytic removal of aqueous Cr(VI) by N-F-Al tri-doped TiO_2

Shuqin Wang†, Yixiao Xie, Weiliang Cheng†, and Jian Gao

School of Environmental Science and Engineering, North China Electric Power University, Baoding, Hebei 071003, P. R. China

(*Received 28 March 2017 • accepted 7 June 2017*)

Abstract−As chromium is a common heavy metal contaminant in water, we have prepared N-F-Al tri-doped TiO_2 catalyst for Cr(VI) removal under visible light. The sample was prepared via a sol-gel method and was characterized by XRD, BET, UV-vis DRS, XPS and SEM techniques. In the photocatalytic experiments, effects of Al/Ti ratio, F/Ti ratio, calcination temperature and different dopants were investigated. The optimum Al/Ti molar ratio, F/Ti ratio and calcination temperature proved to be 0.01, 0.1 and 500 °C, respectively, which is in accordance with the characterization analysis. Catalysts prepared under this condition showed a high photoactivity for Cr(VI) removal in water.

Keywords: Cr(VI), TiO_2, Photocatalytic Reduction, N-F-Al Tri-doping, Al/Ti Ratio, F/Ti Ratio, Calcination Temperature, Different Dopants

INTRODUCTION

Chromium, a common heavy metal contaminant discharged from industrial processes [1], primarily exists in two oxidation states in water: Cr(VI) and Cr(III). The former is considered to be more toxic than the latter and is also more difficult to remove from water [2]. Therefore, reduction methods are usually used to treat chromium containing wastewater [3]. In recent years of pursuing clean and sustainable energy, functional materials [4] and environmentally friendly chemical processes [5-8], photocatalytic reduction method has been gradually used for its high efficiency, low cost, chemical stability and non-toxicity [9-11].

TiO_2 is the most frequently used photocatalyst and is often doped with various nonmetal elements to improve its photoactivity. Nonmetal doping can effectively narrow the band gap and enhance the absorption in visible region. Asahi et al. reported that N-doped TiO_2 had a stronger response to visible light by mixing the N 2p and O 2p states [12]. We prepared N-TiO_2 via a sol-gel method and successfully used it in Cr(VI) removal from water [13,14]. Further, many studies have reported that metal doping has an inhibitory effect on the recombination of electron-hole pairs.

However, most of these studies focused on the photocatalytic degradation of dyes by single or double doped TiO_2 [15,16]; few investigated the removal of Cr(VI) by the multi-nonmetal and metal ions tri-doped TiO_2 nanomaterials under visible light irradiation. We prepared N-F-Al tri-doped TiO_2 via a sol gel method and studied its photocatalytic performance in Cr(VI) removal at a higher concentration (8 mg/L). During the photocatalytic experiments, effects of Al/Ti ratio, F/Ti ratio, calcination temperature and different dopants were investigated. The sample was then characterized by XRD, BET, UV-vis DRS, XPS and SEM techniques. The kinetic mechanism and reusability are also discussed in this paper.

EXPERIMENTAL

1. Materials

Tetrabutyl titanate ($C_{16}H_{36}O_4Ti$), hexamethylenetetramine ($C_6H_{12}N_4$), absolute ethanol (C_2H_5OH), glacial acetic acid (CH_3COOH), ammonium fluoride (NH_4F), aluminum nitrate ($Al(NO_3)_3$) and hydrochloric acid (HCl) were purchased from Tianjin Kemiou Company. All chemicals were analytical grade and employed without any further purification. Potassium bichromate solution was used as the simulated waste water and deionized water was used throughout this experiment.

2. Catalyst Preparation

The preparation of N-F-Al tri-doped TiO_2 was based on a sol gel method according to the literature [8,9]. As we successfully synthesized N-TiO_2 (molar ratio of N/Ti=0.28) in our previous study [13], only Al/Ti and F/Ti ratio varied to find the optimum doping amount. Specifically, 40 ml absolute ethyl alcohol, 0.5 g $C_6H_{12}N_4$ (N sources) and 17 ml tetrabutyl titanate were mixed to form solution A. 40 ml absolute ethyl alcohol, 5 ml glacial acetic acid, 5 ml deionized water and appropriate amount of ammonium fluoride and aluminum nitrate were mixed to form solution B. Next, solution B was slowly dripped into solution A and kept stirred until the gel formed. The resulting gel was then aged for 24 h at room temperature (298 K) and subsequently dried by microwave. Finally, the obtained xerogel was calcined in the muffle furnace for 3 h and ground into powder to get the finial photocatalyst denoted as NFAl-TiO_2. Virgin TiO_2, N-TiO_2 and NF-TiO_2 were prepared via the same method in this study for comparison.

3. Characterizations

The crystal structure of catalysts was examined using X-ray diffraction (XRD) (Y2000, Dandong, China) performed with Cu Kα radiation. The specific surface area and porosity were measured by a Brunauer-Emmett-Teller (BET) analyzer (TriStarII 3020, Mike,

†To whom correspondence should be addressed.
E-mail: wsqhg@163.com, cheng_w_l@163.com
‡This paper is reported in the 11th China-Korea Clean Energy Workshop.

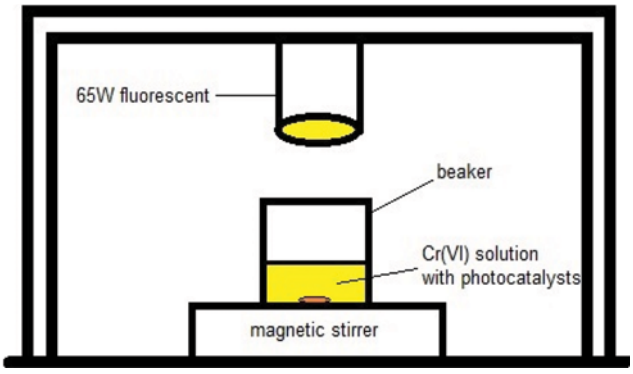

Fig. 1. Schematic diagram of self-made photocatalytic reactor.

USA). The ultraviolet-visible diffuse reflectance spectra (UV-vis DRS) were recorded on a UV-vis spectrophotometer (TU1901, PRISTON, China). XPS techniques (PHI Quantera SXM, ULVACPHI, Japan) was used to analyze the chemical composition of catalysts. Scanning electron microscopy (SEM, KYKY-2800B, China) with a speed voltage of 5 kV was used to observe the microstructure of catalysts.

4. Experimental Procedure

The photocatalytic experiments were on a self-made reactor equipped with a 65 W fluorescent (550 nm) as shown in Fig. 1. To investigate the effects of Al/Ti ratio, F/Ti ratio, calcination temperature and different dopants, the same amount of catalysts (1 g) under different preparation conditions was added into 200 mL Cr(VI) solutions with known concentrations (8 mg/L) at room temperature. Solution pH was adjusted to pH 2.5 with hydrochloric acid before reaction. Then the mixture was kept in darkness for 30 min before 90 min irradiation so as to reach adsorption equilibrium on the surface of catalysts. At constant time intervals, a 10 ml aliquot of the suspensions was withdrawn to measure the instant Cr(VI) concentration using diphenylcarbazide spectrophotometric method (GB 7467-87). The removal efficiency was then calculated by the following formula.

$$\text{Removal Efficiency} = \frac{C_0 - C_t}{C_0} \times 100\% \quad (1)$$

where, C_0 is the initial Cr(VI) concentration and C_t is the instant Cr(VI) concentration. Total chromium was measured by the same method to determine the reduction ratio.

RESULTS AND DISCUSSION

1. XRD Analysis

Fig. 2(a) shows the XRD patterns of virgin TiO_2, N-TiO_2, NF-TiO_2 and NFAl-TiO_2, where the molar ratios of Al/Ti and F/Ti were selected at 0.01 and 0.1 according to the photocatalytic experiments. Compared with virgin TiO_2, there was neither new diffraction peak nor change of the position of the characteristic anatase peak in doped TiO_2, suggesting that N, F and Al doping do not change the crystalline structure of TiO_2. Moreover, the diffraction peak for rutile phase disappeared in all doped TiO_2. The results show that N, F and Al doping have an inhibitory effect on the phase transformation from anatase to rutile, which is in accordance with the results obtained by Giannakas et al. and Chen et al. [17,18]. As anatase phase is expected to have higher photocatalytic activity than rutile phase, these doped TiO_2 are projected to have improved photocatalytic activity.

Further, based on the line-width analysis of the anatase (101) diffraction peak, the average crystal sizes of all these samples, estimated by the Scherrer equation, are summarized in Table 1. As shown, with the increase of dopants, there was a decrease in the crystal size of TiO_2, which proves the inhibitory effect on grain grow by N and F doping [19]. Moreover, insertion of Al into the TiO_2 matrix can hinder the crystallization and agglomeration of TiO_2 crystals during synthesis process, also decreasing the crystal size [20].

Fig. 2(b) shows the XRD patterns of NFAl-TiO_2 samples calcined under different temperatures, including 400 °C, 500 °C and 700 °C. The calcination temperature was of great influence on the crystalline structure and phase composition of the TiO_2. As depicted, the spectrum of NFAl-TiO_2-400 °C and NFAl-TiO_2-500 °C exhibited

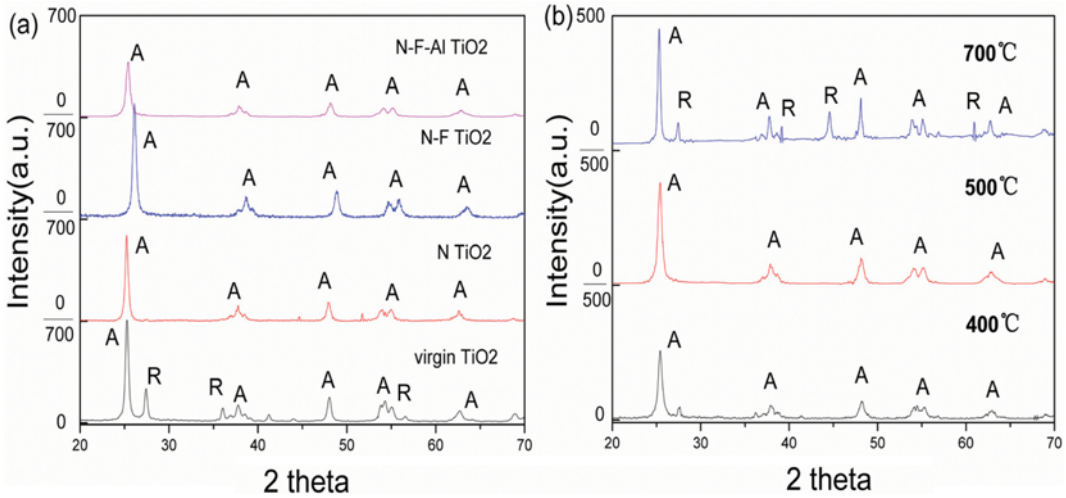

Fig. 2. (a) XRD spectra of virgin TiO_2, N-TiO_2, NF-TiO_2 and NFAl-TiO_2 (b) XRD spectra of NFAl-TiO_2 calcined under different temperature.

Table 1. Phase composition and crystal size of different doped TiO_2

Catalyst	Crystal phase	Crystal size [nm]
Virgin TiO_2-500 °C	A+R	29.8
N-TiO_2-500 °C	A	19.9
NF-TiO_2-500 °C	A	17.2
NFAl-TiO_2-500 °C	A	13.1
NFAl-TiO_2-400 °C	A	17.7
NFAl-TiO_2-700 °C	A+R	45.5

Table 2. BET data foe different doped TiO_2

	S_{BET} [$m^2 \cdot g^{-1}$]	r_p [nm]	V_p [$cm^3 \cdot g^{-1}$]	V_m [$cm^3 \cdot g^{-1}$ STP]
Virgin TiO_2	3.4	9.6	0.008	0.8
N-TiO_2	15.3	8.1	0.031	3.5
NF-TiO_2	17.4	8.6	0.037	4.0
NFAl-TiO_2	19.4	16.1	0.061	4.2

diffraction peaks only for anatase phase, while there were characteristic peaks of rutile phase detected in NFAl-TiO_2-700 °C patterns, denoting that the transformation of the anatase TiO_2 to the rutile TiO_2 occurred. The result is in accordance with the study of Li et al. [21]. Table 1 shows that the smallest crystal size (13.1 nm) was obtained when calcined at 500 °C, suggesting that appropriate calcination temperature can hinder the grain growth. Therefore, the optimum calcination temperature is 500 °C.

2. BET Analysis

Table 2 shows the BET analysis of virgin TiO_2, N-TiO_2, F-TiO_2 and NFAl-TiO_2. The specific surface area of these samples increased in the order: virgin TiO_2<N-TiO_2<F-TiO_2<NFAl-TiO_2. From XRD analysis, the grain sizes decreased with the increase of different dopants. As smaller grain size would lead to a larger specific surface, the result has a good consistency with that of XRD analysis. Therefore, we may conclude that all the three dopants (N, F and Al) are conductive to the dispersion of TiO_2 grains. Further, the largest specific surface area (19.4 m^2/g) was obtained in NFAl-TiO_2, which is nearly six-times the size of virgin TiO_2, suggesting the significant enhancement in adsorption ability.

3. UV-vis DRS Analysis

The UV-vis DRS spectra of virgin TiO_2, N-TiO_2, NF-TiO_2 and NFAl-TiO_2 are presented in Fig. 3(a). As the value of F(R) is proportional to the absorption coefficient, it is used to indicate the light absorption of these samples. Comparing doped catalysts with virgin TiO_2, the light absorption band resulting from electron excitation from valence band to conduction band became broader in the visible region. The intensity of the absorption band varied with the change of dopants and the highest intensity was obtained in NFAl-TiO_2.

To further study the optical properties, band-gap energies (E_g) for all these photocatalysts were calculated by making a plot of $(F(R)h\nu)^{1/2}$ versus hν as shown in Fig. 3(b). The linear part was extended to give the band gap. The estimated E_g values are 3.08, 2.98, 2.93 and 2.72 eV for virgin TiO_2, N-TiO_2, NF-TiO_2 and NFAl-TiO_2, respectively. As E_g values ≤3 eV correspond to visible light absorption, the doped catalysts all can respond to visible light. The results may be associated with the impurity states owing to N-insertion in TiO_2 lattice [22] and the promoting role of F in N-insertion [23]. Moreover, Al injection also leads to a red shift of absorption edge to visible region [24].

4. XPS Analysis

Fig. 4 shows the XPS spectrum of NFAl-TiO_2. The binding energy peaks of Ti_{2p} at 457.8 and 463.6 eV are corresponding to Ti 2p3/2 orbit and Ti 2p1/2 orbit, respectively. The distance between the two peaks is 5.8 eV, suggesting that Ti atoms exist in Ti^{4+} states [25]. The binding energy peak of Al_{2p} is at 73.78 eV, which is accords with the Ti-O-Al structure [20]. It proves some Ti ions are replaced by Al ions in the grain lattice. N_{1s} binding energy is positioned at 398.9 eV, which corresponds to the incorporated interstitial N of Ti-N-O or Ti-O-N [26]. The binding energy of F_{1s} at 682.4 eV also indicated the substitutive F into the TiO_2 grain lattice. Therefore, NFAl-TiO_2 was successfully prepared in this work.

5. SEM Analysis

Fig. 5 shows the morphological images of virgin TiO_2 (left) and NFAl-TiO_2 (right). After doping, these TiO_2 nanoparticles have bet-

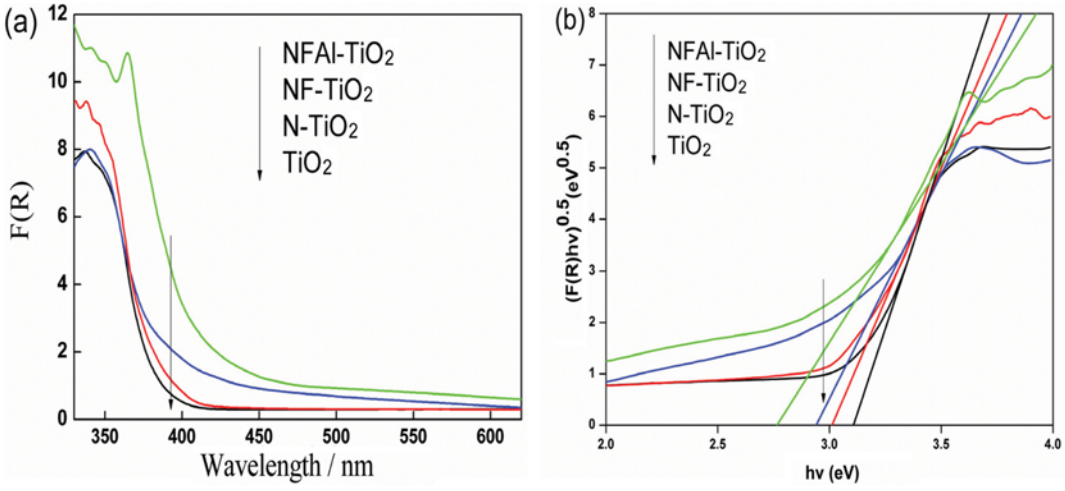

Fig. 3. UV-vis absorption spectra (a) and band gap spectrum (b) of different doped TiO_2.

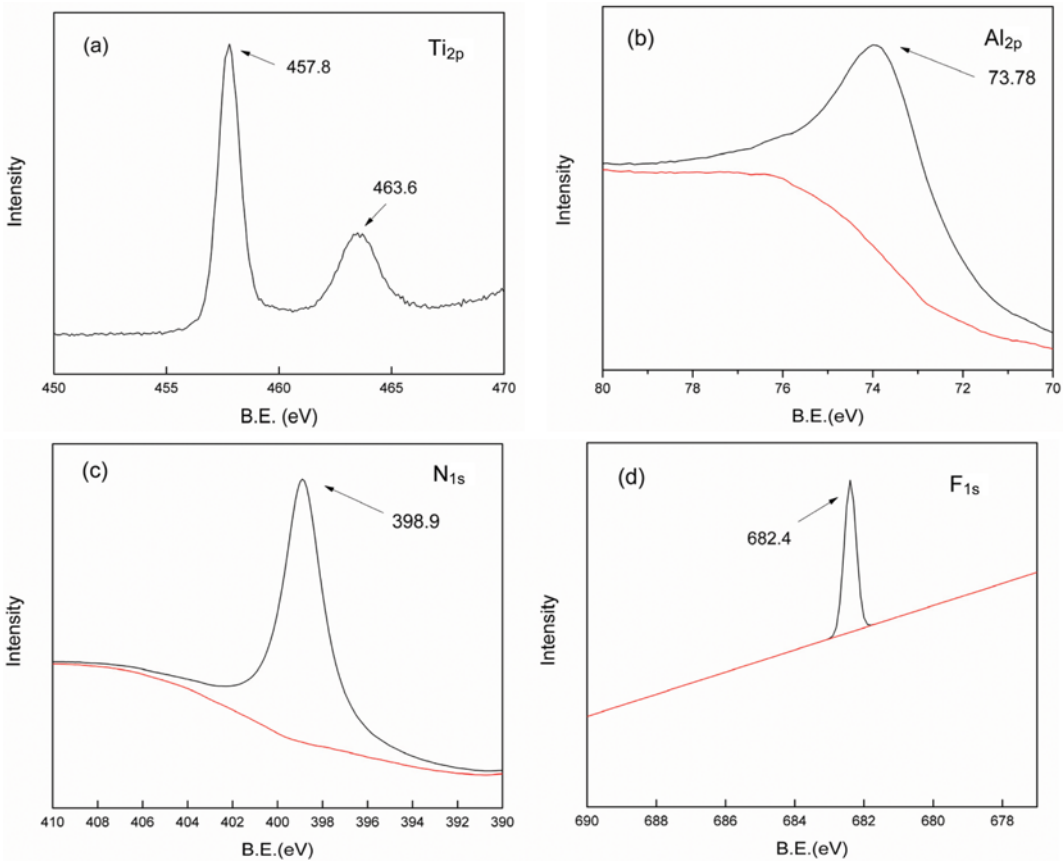

Fig. 4. The binding energy of various elements in NFAl-TiO_2: Ti_{2p} (a), Al_{2p} (b), N_{1s} (c) and F_{1s} (d).

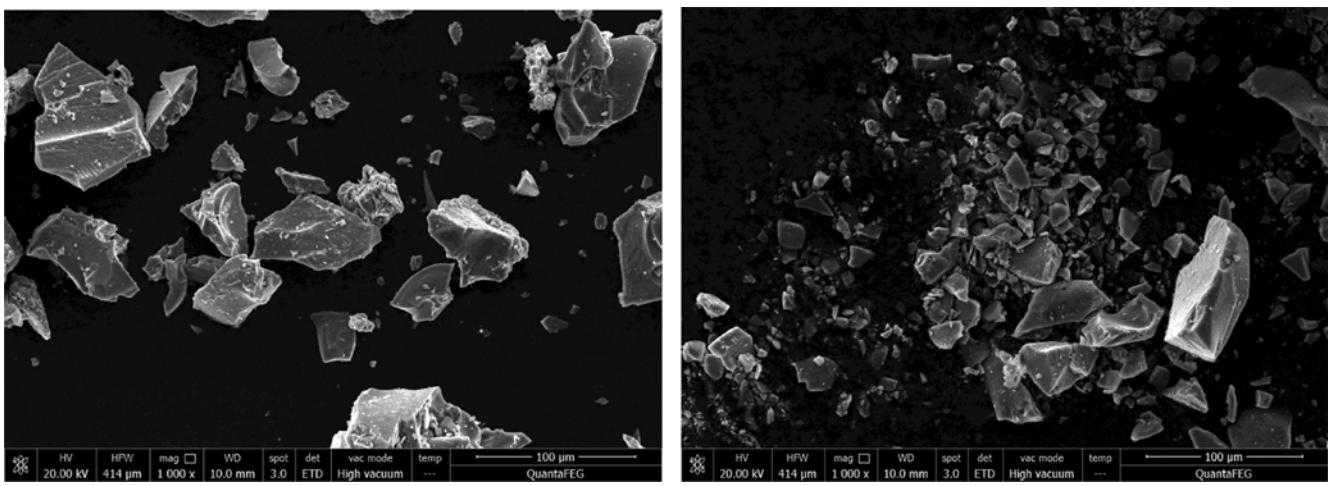

Fig. 5. SEM images of virgin TiO_2 (left) and NFAl-TiO_2 (right).

ter dispersion and smaller grain size. As a result, the specific surface area of NFAl-TiO_2 was greatly increased. The result is in accord with the BET analysis.

6. Photocatalytic Experiments

6-1. Effects of Al/Ti Ratio

Table 3 shows the time profiles of Cr(VI) removal by NFAl-TiO_2 catalysts doped with different concentrations of Al. When the Al/Ti molar ratio increased from 0.002, both the adsorption and pho-

Table 3. Removal efficiency of Cr(VI) by NFAl-TiO_2 catalysts under different Al/Ti molar ratio

	30 min	60 min	90 min	120 min
Al/Ti=0.002	64.8%	73.3%	79.7%	83.9%
Al/Ti=0.006	70.2%	78.9%	85.4%	89.9%
Al/Ti=0.01	80.7%	86.1%	92.4%	96.8%
Al/Ti=0.014	77.4%	83.9%	90.2%	92.8%

Table 4. Removal efficiency of Cr(VI) by NFAl-TiO_2 catalysts under different F/Ti molar ratio

	30 min	60 min	90 min	120 min
F/Ti=0.1	80.7%	86.1%	92.4%	96.8%
F/Ti=0.2	76.6%	81.2%	86.1%	90.9%
F/Ti=0.3	72.5%	77.9%	81.1%	85.3%

Table 5. Removal efficiency of Cr(VI) by NFAl-TiO_2 under different calcination temperature

	30 min	60 min	90 min	120 min
NFAl-TiO_2-400 °C	70.6%	73.1%	75.1%	76.6%
NFAl-TiO_2-500 °C	80.7%	86.1%	92.4%	96.8%
NFAl-TiO_2-700 °C	33.1%	43.5%	51.5%	55.5%

toreduction amount increased and reached the highest point at the ratio of 0.01. After this point, the photoactivity decreased in turn. Thus, 1% is the optimum doping ratio to get a higher photocatalytic activity.

The enhancement is probably owing to the increased surface area and smaller band gap of NFAl-TiO_2 compared to NF-TiO_2 from characterization. Further, Al doping may create lattice defects and then extend the charge carrier's lifetime [20]. However, excessive doping amount of Al may create some recombination centers for electron-hole pairs, thus resulting in a weaker photoactivity [27].

6-2. Effects of F/Ti Ratio

Table 4 shows the time profiles of Cr(VI) removal by NFAl-TiO_2 catalysts doped with different concentrations of F ions. Evidently, appropriate doping amount of F ions increased the removal efficiency of Cr(VI), and the efficiency reached 96.89% at the ratio of 0.1. The result can be explained from two respects. One, the specific surface area and visible light absorption of NF-TiO_2 increased with respect to N-TiO_2 and virgin TiO_2 according to the BET and UV-vis analysis. And two, the highly electronegative fluorine can greatly increase the lifetime of light-induced electrons on the surface of F-TiO_2 [28]. However, as the F doping concentration further increased, it in turn promoted the recombination of electron-hole pairs [29]. Therefore, the optimum F/Ti ratio is proved to be 0.1. Compared with Al doping concentration, it suggests that more nonmetal ions can be inserted into TiO_2 grain lattice than metal ions.

6-3. Effects of Calcination Temperature

Table 5 shows the time profiles of Cr(VI) removal by NFAl-TiO_2 catalysts calcined under different temperatures including 400 °C, 500 °C and 700 °C. As depicted, the removal efficiency improved when the calcination temperature was increased from 400 °C to 500 °C. However, when the temperature further increased to 700 °C, lower removal efficiency was obtained. It is evident that calcination temperature was of great influence on the photoactivity of TiO_2. The result could be explained from the following aspects: (i) within a certain range, higher calcination temperature favors the crystallization process of TiO_2 grains, as well as the removal of residual reactants. The excellent crystallization of NFAl-TiO_2-500 °C subsequently enhanced its photoactivity; (ii) excessive calcination temperature would cause the accumulation of TiO_2 grains, which led to a smaller surface area. Moreover, as calcined under 700 °C, the transformation of anatase phase to rutile phase occurred and the photoactivity declined. Therefore, 500 °C is the optimal calcination temperature for Cr(VI) removal.

6-4. Effects of Different Dopants

Fig. 6(a) shows the time profiles of Cr(VI) removal by TiO_2 catalysts modified with different dopants. Four kinds of catalysts were tested in this section and the removal efficiency increased in the order: TiO_2<N-TiO_2<NF-TiO_2<NFAl-TiO_2. This result can be explained by the fact that N-insertion within the lattice of TiO_2 created defect levels in the band gap, which led to a higher visible light absorption [17]. Moreover, N-doping increased the specific surface area of TiO_2 according to the BET analysis. F ions have a double effect. They can both favor the N-insertion and the formation of reduced Ti^{3+} centers, which could localize the extra electron needed for charge compensation [30]. Finally, appropriate doping amount of Al has an inhibitory effect on the recombination of photo-generated electron-hole pairs [20].

The kinetic profiles of different doped TiO_2 catalysts are shown in Fig. 6(b); the first-order kinetic constants for virgin TiO_2, N-TiO_2, NF-TiO_2 and NFAl-TiO_2 are 0.0029, 0.0032, 0.0035 and 0.021,

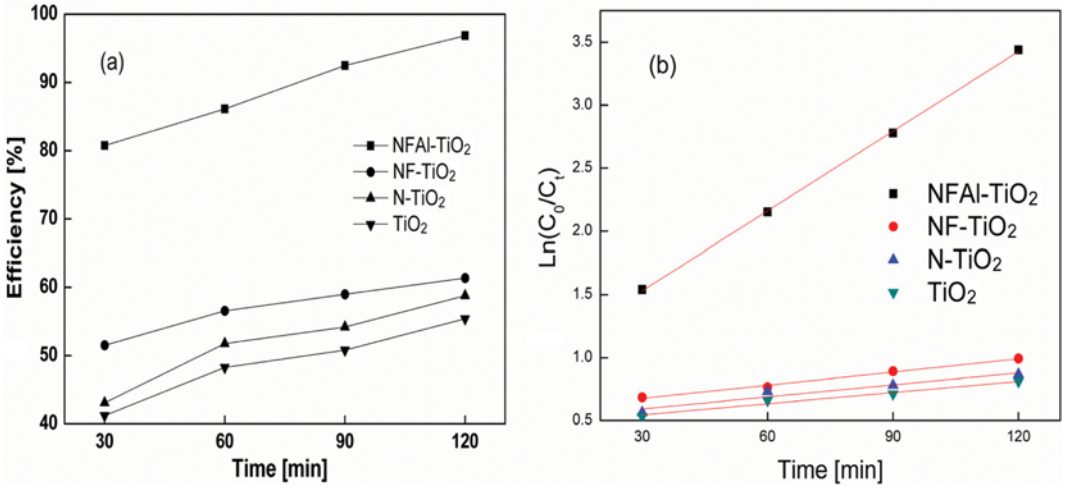

Fig. 6. Cr(VI) removal profiles (a) and kinetic profiles (b) of TiO_2 with different dopants.

Table 6. Photocatalytic performance of different doped TiO_2 after 120 min reaction

	Removal Cr(VI) [μg]	Removal efficiency [%]	Cr(III) amount [μg]	Reduction ratio [%]
TiO_2	886.9	55.4	223.0	25.2
N-TiO_2	941.1	58.8	387.2	41.1
NF-TiO_2	983.4	61.5	420.6	42.8
NFAl-TiO_2	1550.2	96.9	698.4	45.1

respectively. The increased reaction rate for N-TiO_2 and NF-TiO_2 versus virgin TiO_2 is probably attributed to the formation of new energy structure, surfacial Ti^{3+} electrons and $O_2^{\cdot-}$ radicals [18]. As for NFAl-TiO_2 catalyst, the decreased recombination rate of electron-hole pairs by Al doping also promoted the photoreduction of Cr(VI). Therefore, the photocatalytic reaction rates for these catalysts increase in the same order with Fig. 5(a).

The amount of reduced Cr ions and reduction rate are calculated in Table 6. As there was a certain amount of Cr(III) ions adsorbed on TiO_2, we only detected the reduced Cr(III) ions in water, which is less than the removed Cr(VI) ions. From the table, both the adsorption process and the photoreduction process were promoted owing to the great increase in the specific surface area and visible light absorption of TiO_2 after doping. The results prove that NFAl-TiO_2 has the highest photoactivity for Cr(VI) removal.

7. Efficiency under Different Initial Cr(VI) Concentration

Fig. 7 shows the Cr(VI) removal profiles by N-TiO_2 and NFAl-TiO_2 under different initial Cr(VI) concentration. As there are finite adsorption sites on the surface of TiO_2, the removal efficiency declined with the increase of Cr(VI) concentration. Therefore, the specific surface area is critical to the result of treatment. Comparing the two catalysts, the superior photoactivity of NFAl-TiO_2 is probably owing to its larger surface, as well as the better light absorption. More importantly, the efficiency stood above 70% at the initial concentration of 20 ppm. It is evident tri-doped TiO_2 has

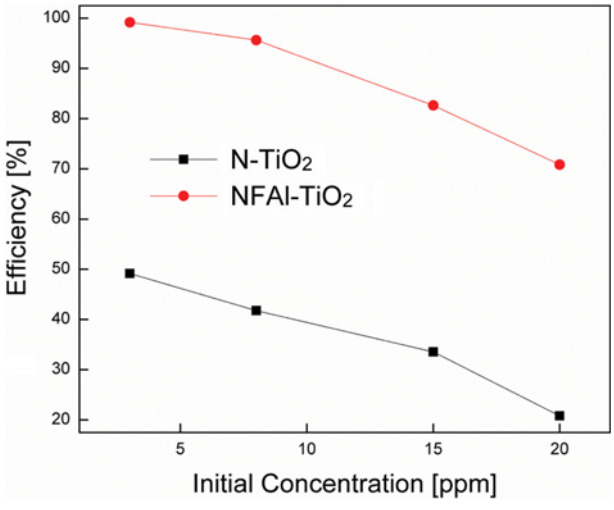

Fig. 7. Cr(VI) removal by N-TiO_2 and NFAl-TiO_2 under different initial Cr(VI) concentration.

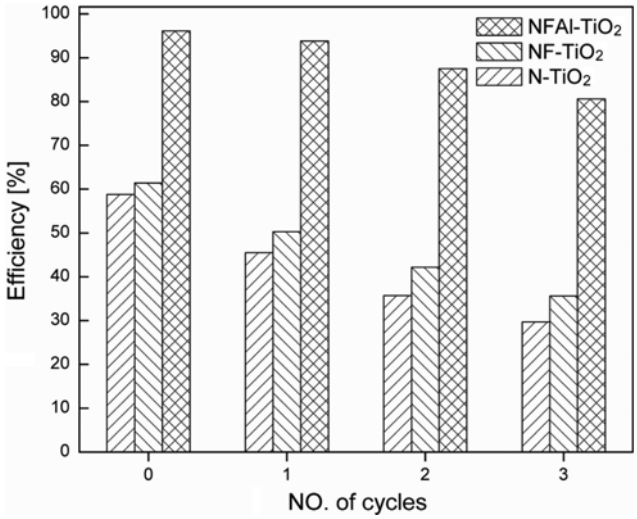

Fig. 8. Reusability of N-TiO_2, NF-TiO_2 and NFAl-TiO_2 for Cr(VI) removal.

many more advantages for Cr(VI) treatment.

8. Reusability

The stability and reusability of catalysts are important factors for industrial application from the point of energy saving. In this section, the reacted solution was filtered and the precipitate was washed with deionized water for several times. After subsequent drying, the recollected catalysts were employed for a fresh Cr(VI) solution. Fig. 8 shows the removal efficiency of Cr(VI) by doped TiO_2 under different cycle numbers. As depicted, the efficiency by NFAl-TiO_2 stood above 80% after three repeated cycles, much higher than the other catalysts. Therefore, NFAl-TiO_2 is an appropriate photocatalyst for Cr(VI) removal from water.

CONCLUSIONS

Virgin TiO_2, N-TiO_2, NF-TiO_2 and NFAl-TiO_2 photocatalysts prepared by sol-gel method were characterized and applied for the photoreduction of Cr(VI) in water. From XRD, pure anatase phase was formed in all doped catalysts, and NFAl-TiO_2 calcined under 500 °C had the smallest grain size. BET analysis proved the largest specific surface area obtained by NFAl tri-doping. In the UV-vis DRS analysis, a narrowing of E_g values was observed for all doped catalysts, and NFAl-TiO_2 has the smallest band gap width. XPS analysis indicates that N, F and Al ions were successfully inserted into TiO_2 grain lattice.

The photocatalytic experiments showed that (i) to enhance the photocatalytic performance of NFAl-TiO_2, the optimum Al/Ti and F/Ti molar ratios were 0.01 and 0.1, respectively. Best calcination temperature proved to be 500 °C; (ii) with respect to virgin TiO_2, an increase in Cr(VI) removal efficiency was observed in all doped cases. The highest efficiency was obtained by NFAl-TiO_2; (iii) NFAl-TiO_2 had the fastest photocatalytic reaction rate and the best reusability.

ACKNOWLEDGEMENTS

This work was financially supported by National Natural Sci-

ence Foundation of China (Grant No. 51476056) and Natural Science Foundation of Hebei (No. E2014502111).

REFERENCES

1. Y. Gao and J. Xia, *J. Environ. Sci. Technol.*, **45** , 8605 (2011).
2. P. Miretzkya and A. Fernandez Cirelli, *J. Hazard. Mater.,* **180**, 1 (2010).
3. E. C. Barrera-Díaz, L. L. Violeta and B. Bilyeu, *J. Hazard. Mater.*, **223-224**, 1 (2012).
4. P. He, Z. L. Hou, C. Y. Wang, J. L. Zhong, J. Jian and B. Song, *Ceram. Int*., **43**, 262 (2016).
5. X. Y. Zhang, H. S. Chen and D. N. Fang, *J. Solid State Electrochem.*, **20**, 2835 (2016).
6. Y. H. Bao, X. Y. Zhang, X. Zhang, L. Yang, X. Y. Zhang, H. S. Chen, M. Yang and D. N. Fang, *J. Power Sources*, **321**, 120 (2016).
7. X. Y. Zhang, L. Yang, F. Hao, H. S. Chen, M. Yang and D. N. Fang, *Nanomaterials*, **5**, 1985 (2015).
8. X. Y. Zhang, F. Hao, H. S. Chen and D. N. Fang, *Mech. Mater.*, **91**, 351 (2015).
9. Q. Wang, X. D. Shi, J. J. Xu, J. C. Crittenden, E. Q. Liu, Y. Zhang and Y. Q. Cong. *J. Hazard. Mater.*, **307**, 213 (2016).
10. R. Djellabi, F. M. Ghorab, S. Nouacer, A. Smara and O. Khireddine, *Mater. Lett.*, **176**, 106 (2016).
11. X. F. Fu, H. P. Yang, G. H. Lu, Y. M. Tu and J. M. Wu, *Mater. Sci. Semicon. Proc.,* **39**, 362 (2015).
12. R. Asahi, T. Morikawa, T. Ohwaki, K. Aoki and Y. Taga, *Science*, **293**, 269 (2001).
13. S. Q. Wang and D. L. Zhang, *Adv. Mater. Res.*, **610-613**, 1497 (2013).
14. S. Q. Wang, W. B. Liu, P. Fu and W. L. Cheng, *Korean J. Chem. Eng.*, **34**(5), 1584 (2017).
15. A. E. Giannakas, M. Antonopoulou, C. Daikopoulos, Y. Deligiannakis and I. Konstantinou, *Appl. Catal. B-Environ.*, **184**, 44 (2016).
16. R. Fagan, D. E. McCormack, S. Hinder and C. Suresh, *Mater. Des.,* **96**, 44 (2016).
17. X. Y. Chen, D. H. Kuo and D. F. Lu, *Chem. Eng. J.*, **295**, 192 (2016).
18. S. Cao, H. Q. Wang, F. X. Yu, M. P. Shi, S. Chen, X. L. Weng, Y. Liu and Z. B. Wu, *J. Colloid Interface Sci.*, **463**, 233 (2016).
19. A. E. Giannakas, E. Seristatidou, Y. Deligiannakis and I. Konstantinou, *Appl. Catal. B-Environ*., **132-133**, 460 (2013).
20. W. J. Zhang, X. B. Pei, J. L. Chen and H. B. He, *Mat. Sci. Semicon. Proc.,* **38**, 24 (2015).
21. D. Li, X. W. Cheng, X. J. Yu and Z. P. Xing, *Chem. Eng. J.*, **27**, 9994 (2015).
22. D. Li, H. Haneda, S. Hishita and N. Ohashi, *Chem. Eng. J.,* **17**, 2588 (2005).
23. C. D. Valentin, E. Finazzi and G. Pacchioni, *Chem. Eng. J.,* **20**, 3706 (2008).
24. D. D. Yu, W. Zhou, Y. Y. Liu and P. Wu, *J. Magn. Magn. Mater.,* **404**, 7 (2016).
25. J. Xiao, Z. C. Pan, B. Zhang, G. Liu, H. C. Zhang, X. F. Song, G. H. Hu, C. M. Xiao, Z. G. Wei and Y. Y. Zheng, *Mater. Lett.*, **188**, 66 (2017).
26. O. Elbanna, P. Zhang, M. Fujitsuka and T. Majima, *Appl. Catal. B-Environ*., **192**, 80 (2016).
27. S. Y. Liu, Q. G. Feng and W. H. Tang, *Chin. J. Inorg. Chem.,* **27**, 673 (2011).
28. EM Samsudin, SBA Hamid, JC Juan, JB Wan, G Centi, *Appl. Surf. Sci.*, **370**, 380 (2016).
29. W. Yua, X. J. Liub and L. K. Pan, *Appl. Surf. Sci.,* **319**, 107 (2014).
30. A. M. Czoska, S. Livraghi, M. Chiesa, E. Giamello, S. Agnoli, G. Granozzi, E. Finazzi, C. D. Valentin and G. Pacchioni, *J. Phys. Chem. C.*, **112**(24), 8951 (2008).